scientific reports

Check for updates

OPEN

Influence of biochar on the partitioning of iron and arsenic from paddy soil contaminated by acid mine drainage

Chipeng Zhang[1,2]✉, Jianglan Luo[1], Wansheng Song[1], Han Chen[1] & Shunyuan Zhang[1]

Paddy fields contaminated by arsenic-containing acid mine drainage (AMD) may also have rich iron in soil. Whether this iron can be loaded onto biochar to passivate the dissolved arsenic is worth further exploration. Soil was mixed with biochar prepared at 400, 550, and 700 °C and incubated under alternating anaerobic and aerobic conditions. Soil, soil solution and biochar samples were analysed using ICP-MS, FTIR, SEM, XPS, etc. The results showed that biochar prepared at lower pyrolysis temperatures contained a higher number of functional groups. Under the combined action of microorganisms, primarily from the Firmicutes phylum, biochar promoted the dissolution of arsenic-containing iron oxides in soil, with the residual arsenic also undergoing transformation. The biochar rapidly loaded dissolved iron onto its surface, likely in the form of Fe_3O_4 and FeOOH, and adsorbed arsenic primarily as As(III). Although the iron oxides detached over time, they were more stable on the biochar prepared at 400 °C compared to those prepared at higher pyrolysis temperatures. Meanwhile, the arsenic content on the biochar increased, raising the As/Fe molar ratio to above that of the soil. This study lays the foundation for further exploring the long-term use of biochar in AMD-contaminated paddy fields.

Keywords Biochar, Paddy field, Mining activity, Iron oxides, Arsenic

Mining activities are some of the most environmentally destructive anthropogenic practices and have led to excessive levels of metal(loid)s in soil. Arsenic (As) contamination has attracted worldwide attention in recent years due to its significant threat to the agricultural product quality and human health[1,2]. Arsenic exposure through the food chain can cause disorders of the blood vessels, reproductive system and nervous system[3]. The application of stabilisation agents to soil is a commonly used As remediation technology. Among various materials, biochar has attracted increasing interest due to its widespread sources, low cost and high stability. Biochar contains alkaline salts, a substantial amount of dissolved organic carbon (DOC) and oxygen-containing functional groups, and has a high specific surface area and porous structure[4]. All of these physiochemical properties can change the environmental conditions of soil and influence the partitioning of As between solid and liquid phases.

The application of biochar to soil has the potential to enhance the release of As, especially in paddy fields. The porous structure of biochar is one of its most attractive features due to its ability to increase soil porosity[5]. This may improve soil's water-holding capacity and decrease the solid-liquid ratio. The addition of water helps to enhance the dissolution of soil minerals and release trace elements, including heavy metals. Biochar also has a liming effect because it contains negatively charged groups such as hydroxyl and carboxyl groups, which can react with $H^{[+6}$. As soil pH increases, mineral particle surfaces will have greater negative charges and their ability to adsorb anion ions like $HAsO_4^{2-}$ and $HAsO_3^{2-}$ will be weakened[7]. This will also promote the release of As into soil solution. Additionally, some biochar functional groups—particularly hydroxyl (OH^-) groups—can act as electron donors[8]. The functional groups of biochar vary with different pyrolysis temperatures, which can influence the bioavailability of As[9]. Biochar can also provide organic carbon to promote anaerobic microbial activity[10], leading to a reduction of oxidising minerals in the soil. It has been reported that biochar can decrease redox potential (Eh) to − 300 mV and enhance the release of iron (Fe) and As[11,12].

[1]College of Resources and Environmental Engineering, Key Laboratory of Karst Georesources and Environment, Ministry of Education, Guizhou University, Guiyang 550025, China. [2]Guizhou Karst Environmental Ecosystems Observation and Research Station, Ministry of Education, Guizhou University, Guiyang 550025, China. ✉email: Re.cpzhang@gzu.edu.cn

However, as raw biochar cannot generally be used as an amendment agent for As-contaminated paddy fields, biochar is modified to improve its ability to passivate As. One modification method is to impregnate its surface with metal oxides, of which iron oxide has attracted the most attention[13]. This is because iron oxide is environmentally friendly and can sequester As through inner-sphere complexation on its surface[14]. Wu et al.[15] showed that the application of iron-modified biochar to soil can increase microbial diversity, but the relative abundance of different species may be positively or negatively affected[16,17]. However, variations in the microbial community do not affect the ability of biochar to remediate As-contaminated paddy fields. Furthermore, it has been shown that modified biochar can significantly reduce the bioavailability of As and its content in rice grains[18,19]. Functional groups such as C = O can also decrease the bioavailability of As by acting as electron acceptors to oxidise As(III) to the less mobile As(V)[20]. Once As is immobilised in the pores of biochar, its stability increases. Even though iron oxides in soil shift between amorphous and crystalline phases, their ability to adsorb dissolving As does not change significantly.

Acid mine drainage (AMD) is a common source of pollution from mining activity and contributes greatly to soil contamination. AMD is mainly generated from the oxidation of pyrite (FeS_2). Its features include a low pH and high concentrations of sulphate, heavy metals and metalloids[21]. AMD into farmland leads to significant physiochemical changes, including soil acidification, heavy metal enrichment and alterations to the microbial community[22]. In terms of metal enrichment, Fe generally increases the most. This usually results in the generation of (hydro)oxides such as ferrihydrite, goethite and hematite, which are reduced by dissimilatory iron-reducing bacteria under anaerobic conditions to release large amounts of ferrous ions (Fe(II)) into soil solution[23]. These cations can be readily adsorbed by the negatively charged functional groups of biochar[24], as in the preparation process of iron-modified biochar described previously[25], and are oxidised to Fe(III) under aerobic conditions. Based on the above understanding, we hypothesised that biochar could load iron oxides and effectively immobilise As in AMD-contaminated paddy fields with fluctuating redox conditions.

The objectives of this study were to (1) investigate the impact of biochar application on soil properties with changes in anaerobic and aerobic conditions, (2) to understand the effect of biochar on soil Fe and As transformation and release, and (3) to elucidate the partitioning process of the two elements on the biochar surface. The research results will provide insight into the use of biochar for As immobilisation in AMD-contaminated paddy fields.

Materials and methods

Preparation of soil and biochar

Soil samples were collected from paddy fields near a high-As coal mine in Jiaole, Guizhou Province, southwest China. The soil at this site had been acidified by AMD, and its pH was about 4.8. Its Fe content was about 82 g kg^{-1}, and its As content was about 65 mg kg^{-1}, which exceeded China's standard for soil (GB 15618-2008) (30 mg kg^{-1}). This has influenced rice grain quality in the area[26]. The soil texture was silty clay loam. Other soil characteristics were described in our previous publication[27]. The samples were air-dried and then crushed to a particle size of < 0.4 mm for incubation experiments.

Eupatorium adenophorum is an invasive species in the study area. It was dried in an oven at 60 °C and used to prepare raw biochar in a tubular carbonisation furnace. The pyrolysis temperature was a key parameter in biochar production. *Eupatorium adenophorum* biochar is typically produced within the temperature range of 300–700 °C[28,29]. If the temperature is too high, the biochar surface may lack functional groups. Additionally, the biochar produced at 300 °C is nearly neutral[30] and does not provide advantages for remediating acidified soil caused by AMD. Therefore, the pyrolysis temperatures of 400 °C, 550℃, and 700 °C were selected for this study. The residence time in the reactor was 4 h, and the heating rate was 2.5 °C min^{-1}. The biochar produced at the different pyrolysis temperatures was denoted BC-400, BC-550 and BC-700. The biochar was washed with ultrapure water before use to remove ash and soluble components.

Incubation experiment

Figure 1 presents a schematic diagram of the experimental setup, which was adopted to conduct a series of bench-scale soil incubation experiments. The apparatus was a columnar Perspex reactor with a diameter of 12 cm, a height of 21 cm and a sealing cover at the top. A stirrer, pH and Eh probes, and an exhaust valve were installed on it. One aeration disk was set at the bottom and connected to nitrogen and oxygen cylinders. The sampling port was located at the lower part of the cylinder.

Portions of soil (30 kg) were mixed thoroughly with one of the biochar samples

According to our pot experiment[31], the biochar application rate was 3% (w/w). They were then placed into the setup. Based on the biochar used, the experiments were divided into the BC-400, BC-550 and BC-700 groups, and a control group (CK) without biochar was also included. Additionally, ultrapure water was added in a solid-liquid ratio of 5:6, and the resulting suspension was stirred at 100 rpm. Nitrogen and oxygen were injected in sequence to create an anaerobic or aerobic environment, with each period lasting for 15 days. The entire experiment spanned 75 days, including three anaerobic periods (0–15 d, 30–45 d and 60–75 d) and two aerobic periods (15–30 d and 45–60 d). The pH and redox potential (Eh) were measured using portable parameter instruments. Each treatment was performed in triplicate.

Sample collection and determination

Aliquots of the soil suspension were collected into centrifuge tubes at the end of each period (15, 30, 45, 60 and 75 d). These samples were centrifuged at 5000 rpm for 20 min and the soil solution was filtered into centrifuge tubes through a 0.45 μm filter membrane for the determination of total Fe, Fe(II), As and DOC. The remaining soil and aged biochar samples were separated by the flotation method[32]. The soil was freeze-dried to a constant weight and ground through a 200-mesh quasi-sieve to determine the Fe and As content and the As form. The

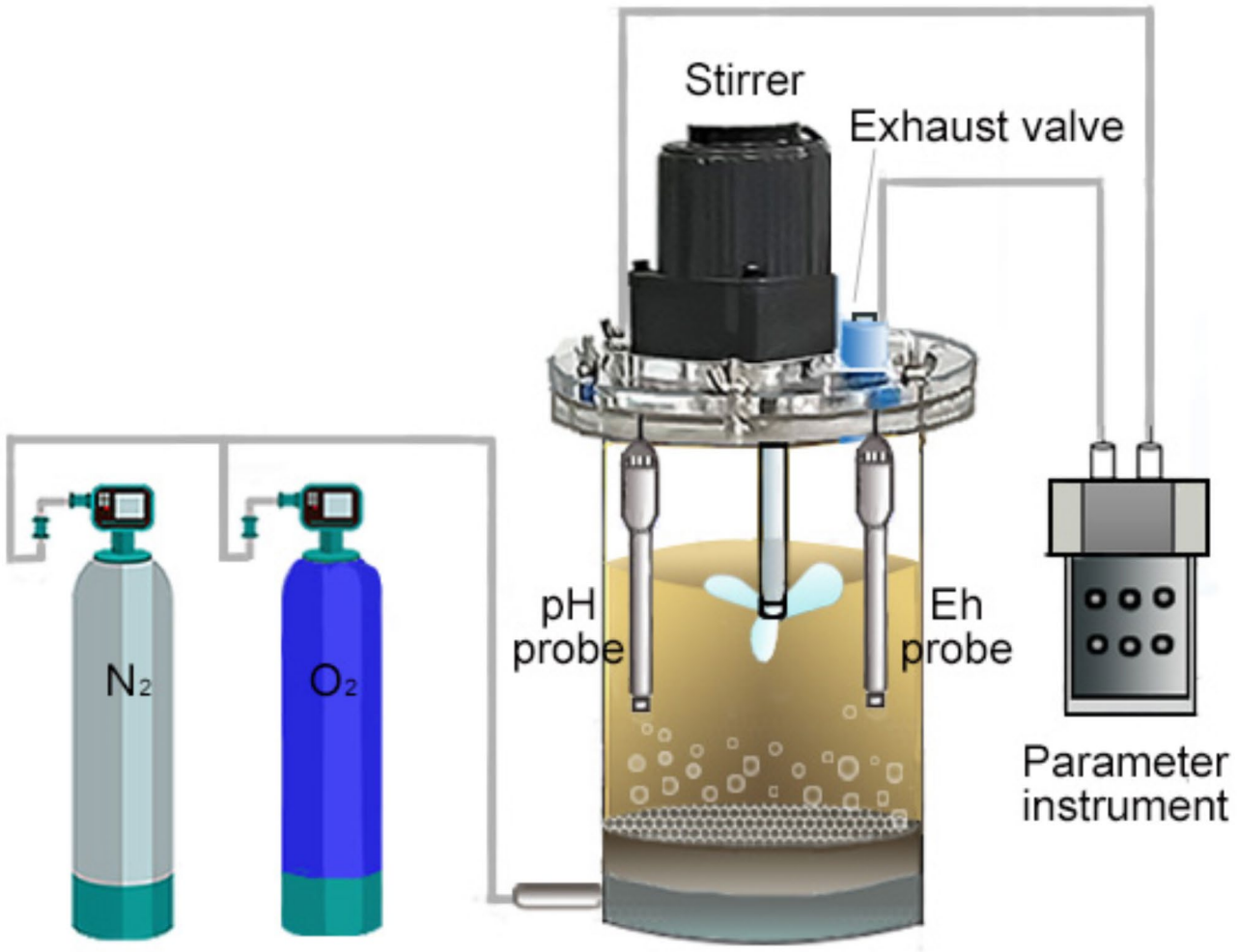

Fig. 1. Experimental setup for soil incubation.

biochar was washed using ultrapure water to remove soil adhered to its surface for the analysis of Fe and As content, surface morphology and chemistry. Additionally, samples of fresh soil suspension were collected in the second anaerobic and aerobic periods for the analysis of microorganisms.

The concentrations of total Fe and As in soil solution were determined by flame atomic absorption spectrophotometry (FAAS) and inductively coupled plasma mass spectrometry (ICP-MS), respectively. The concentration of Fe(II) was determined by the phenanthroline spectrophotometric method. The DOC was analysed using a total organic carbon analyser (TOC-5000 A). The Fe and As content in soil and biochar were determined using the above methods after digestion with aqua regia. The form of As in the soil was determined by the modified Wenzel's method[33] and was classified as non-specifically bound (F1), specifically bound (F2), amorphous and poorly crystalline hydrous oxides (F3), well-crystallised hydrous oxides (F4) and residual phase (F5). The microbial population structure in soil was investigated using high-throughput sequencing of 16 S rRNA[34]. The microbial biomass carbon (MBC) was measured via the substrate-induced respiration method[35]. Fourier transform infrared spectroscopy (FTIR) was used to analyse the chemical properties of the raw biochar. Scanning electron microscopy (SEM) was used to investigate the morphology of the aged biochars and X-ray photoelectron spectroscopy (XPS) was used to determine their surface chemical properties.

Data processing

The XPS results were fitted using Avantage 5.9, where the standard peak for fitting the C1s spectrum was set at 284.8 eV. The data from triplicates were averaged and standard deviations (SD) were calculated. Pearson correlation analysis ($p < 0.05$) was carried out to examine the relationship between different indicators. The figures were produced using Origin 2021.

Results and discussion

Variation of environmental conditions

There were similar variation characteristics of the pH, Eh and DOC concentrations in soil suspensions among groups during the anaerobic/aerobic periodic experiments (Fig. 2). The pH of the CK group was about 5.4 at

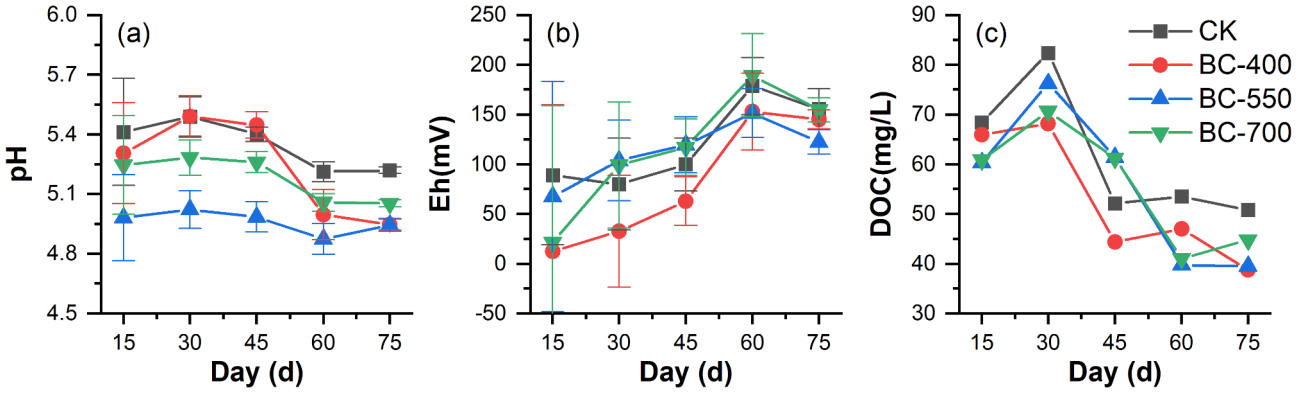

Fig. 2. (**a**) pH, (**b**) Eh and (**c**) DOC concentration in CK, BC-400, BC-550 and BC-700 with experimental time.

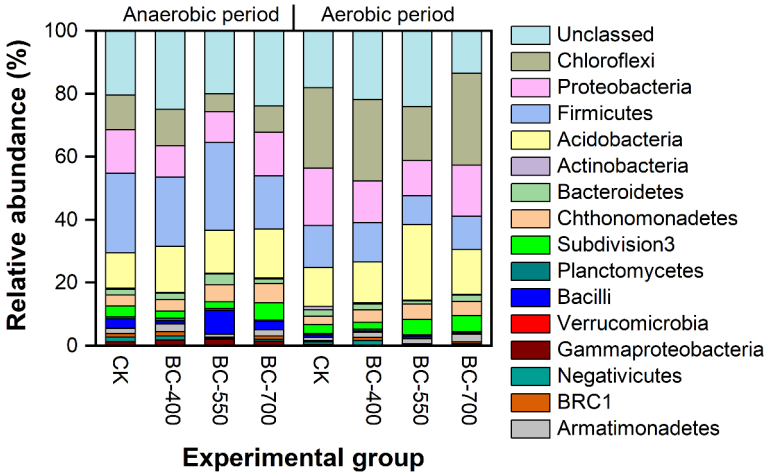

Fig. 3. Microbial community composition and relative abundance at the phylum level in the anaerobic and aerobic periods of each group.

0–45 d, decreased to 5.2 after the following aerobic period and changed minimally after the final anaerobic period. The BC-400 group also experienced a significant decrease in pH after the second aerobic treatment and was about 0.2 lower than the CK group, on average. The pH of both the BC-550 and BC-700 groups was lower than that of the CK group throughout the entire experimental process, with the lowest pH being that of the BC-550 group.

The Eh in each group showed an overall increasing trend during the experiment. The Eh ranged from 80 to 179 mV in the CK group. The Eh of the BC-400 group was consistently lower than that of the CK group, with a minimum of 12 mV. Usually, iron oxides undergo reductive dissolution when the redox potential is below 200 mV and As is also released[36]. The DOC concentration in soil solution showed a decreasing trend in each group, which indicated that DOC was continuously decomposed by microorganisms during the experiment. Except for at 45 d, the DOC concentration in each BC group was lower than that in the CK group and the BC-400 group was lowest at about 8.61 mg L^{-1}. This was because the cleaned biochar did not release DOC and probably had a certain adsorption effect[37].

The amount of soil microbial biomass can be reflected by the MBC. The analysis results showed that the MBC of the CK group was approximately 379 mg kg^{-1} (dry soil) at the end of the experiment, while the MBC of the BC-400, BC-550 and BC-700 groups decreased by about 76 mg kg^{-1} (dry soil), 6 mg kg^{-1} (dry soil) and 183 mg kg^{-1} (dry soil), respectively. After anaerobic treatment, the main microbial species in each group were similar at the phylum level, including Proteobacteria, Firmicutes, Acidobacteria and Chloroflexi with relative abundances greater than 10%, followed by Bacilli, Chthonomonadetes etc. (Fig. 3). Proteobacteria genera *Geobacterium* and *Shewanella* are typical dissimilatory iron-reducing bacteria[38]. The *Clostridium* genus of Firmicutes also has iron-reducing ability and the arrA gene it carries also reduces As[23]. Additionally, the Acidobacteria phylum also contains iron-reducing bacteria[39]. After the aerobic treatments, the microbial species of each group did not change at the phylum level. However, the relative abundance of Firmicutes decreased significantly, while the relative abundance of Proteobacteria and Chloroflexi increased. There was a significant negative correlation

between the relative abundance of Firmicutes and Chloroflexi (r = -0.80, $p < 0.05$). The Proteobacteria genera *Alphaproteobacteria* and *Betaproteobacteria* have Fe(II) oxidation ability[40].

Promoting effect of biochar on iron and arsenic release

The environmental behaviour of As in soil is closely related to the presence of iron oxides. Throughout the entire experimental process, the Fe concentration in soil solution showed high and low periodic variations under anaerobic/aerobic operations, respectively (Fig. 4a). In the first anaerobic period (0–15 d), the total Fe concentration in soil solution ranged from 45.30 to 69.60 mg L^{-1} with the main speciation being Fe(II). Although the BC-400 group had the lowest Eh, its Fe concentration was not significantly higher than that of the CK group; however, in the second anaerobic period (30–45 d), the BC-400 group had the highest Fe concentration, followed by the BC-550 group. The Fe concentration of the BC-700 group was slightly higher than that of the CK group. These results indicated that after a certain period of interaction between biochar and soil, iron release was significantly enhanced. It was also observed that the lower the pyrolysis temperature of the biochar, the greater the Fe release. The analysis of the relationship with microorganisms revealed a positive correlation between Fe(II) concentration and the relative abundance of Firmicutes ($r = 0.61$, $p = 0.11$) during the second anaerobic and aerobic periods, while a significant negative correlation was observed with the relative abundance of Proteobacteria (r = -0.76, $p < 0.05$). This suggested that Firmicutes might play a key role in the reductive dissolution of iron oxides, while Proteobacteria likely catalysed the dissimilatory oxidation of Fe(II), promoting the formation of iron oxide precipitates.

The As concentration in soil solution also showed periodic variations with experimental conditions. It decreased after entering the aerobic period (Fig. 4b) and was significantly positively correlated with Fe concentration ($r = 0.66$, $p < 0.01$). In the first anaerobic period, As release was relatively weak and the concentration was between 6.06 and 9.43 μg L^{-1}, with little difference among the groups. The average As/Fe concentration ratio was 1.2×10^{-4}. The As concentration in the second anaerobic stage was about 2 to 4 times that in the first stage and the As concentrations of the three BC groups—especially BC-400 and BC-550—were higher than that of the CK group. This was because biochar could serve as an electron donor and shuttle to promote iron oxide dissolution and As release[23]. During this stage, the As/Fe concentration ratio increased to about 4.5×10^{-4}. The As concentration continued to decrease after the experiment progressed into the third anaerobic period (60–75 d). This may have been related to the continuous consumption of DOC (Fig. 2c), which weakened the reduction of iron oxides. Additionally, under anaerobic conditions, Fe(II) would have been oxidised by iron-oxidising bacteria to generate secondary minerals such as ferrihydrite, with which As would have coprecipitated[41].

The DOC and functional groups contained in biochar can influence microbial activity and soil mineral transformation[10]. The biochar did not increase the DOC concentration in soil solution because of the pretreatment (Fig. 2c). As described above, the soil microbial biomass carbon and population structure of the BC-400 and BC-550 groups were similar to those of the CK group, suggesting that their higher Fe release during the second anaerobic period may not have been solely influenced by iron-reducing bacteria. Although the microbial biomass of the BC-700 group was about half that of the CK group, the difference in Fe concentration between the two groups was relatively small, which further confirmed this point. It is speculated that the different Fe release levels between the BC and CK groups may be related to the differences in the functional groups of the biochar.

The results of biochar FTIR analysis are shown in Fig. 5. Compared with BC-700, BC-400 and BC-550 contained more functional groups. The characteristic peaks were mainly concentrated in the wavenumber range of 750 to 3500 cm^{-1}, indicating the presence of various functional groups on the biochar surfaces. Hydroxyl groups exhibit stretching vibrations at 3420 cm^{-1}, C-H at 2920 cm^{-1}, C = C group at 2360 $cm^{[-1}$ and C = C/C = O

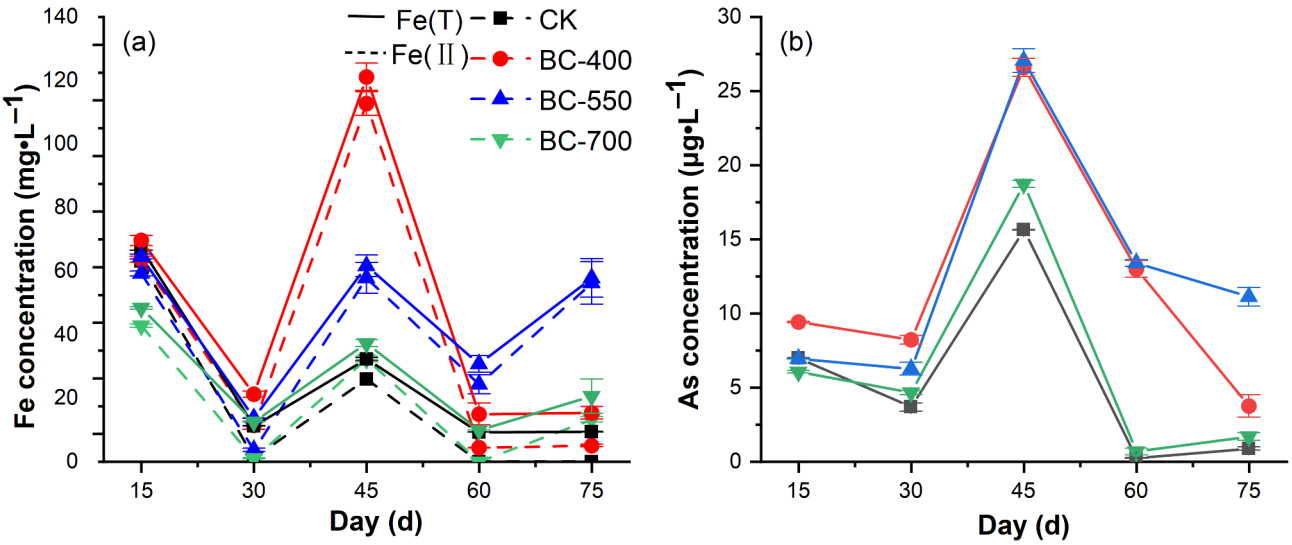

Fig. 4. Changes in (**a**) iron and (**b**) arsenic concentrations in soil solution across CK, BC-400, BC-550 and BC-700 over experimental time.

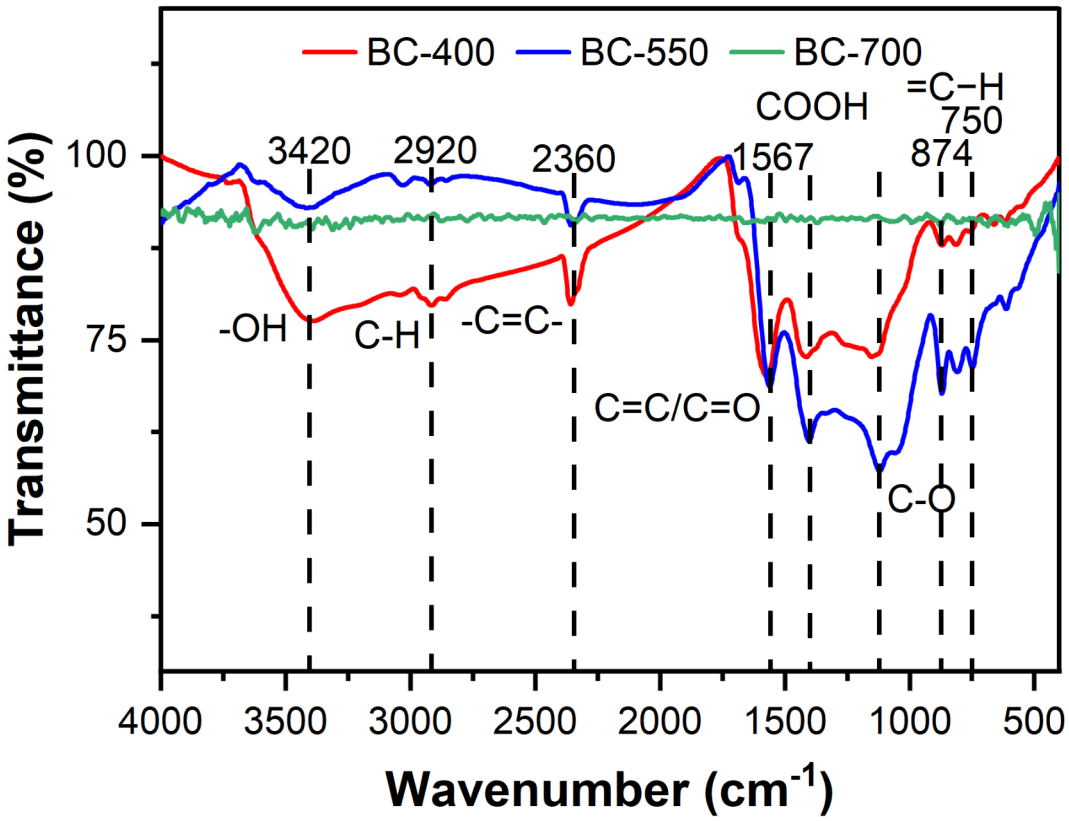

Fig. 5. FTIR spectrum of biochar, including BC-400, BC-550 and BC-700, before interaction with soil.

on the aromatic ring at 1567 cm[−1][10,42–44]. This indicated that the biomass was not fully carbonised after pyrolysis and there were many aromatic compounds in BC-400 and BC-500. Therefore, they likely contained phenolic and alcohol compounds, with the oxygen atoms in the hydroxyl groups serving as electron donors[45,46]. The graphite-like aromatic structures could also serve as electron shuttles[47], thereby promoting the reduction and dissolution of Fe(III) minerals. Kappler et al.[48] and Xu et al.[49] also found that biochar promotes the dissolution of weakly crystalline iron oxides (ferrihydrite) and crystalline iron oxides (haematite). As the pyrolysis temperature increased, the number of electron donors contained in the biochar decreased[50]; this resulted in a significant decrease in Fe release for the BC-700 group compared with the other two BC groups.

Analysis of arsenic transformation in soil

The content and form of As in the soil were influenced by the interaction between biochar and soil (Fig. 6). Compared with the CK group, the As content in the soil of all three BC groups decreased at the end of the experiment. The lower the pyrolysis temperature, the lower the As content in the soil, with a decrease of approximately 10.5 mg kg^{-1} in the BC-400 group compared with the CK group. The large specific surface area and abundant functional groups of biochar meant that it not only promoted the reduction and dissolution of As and Fe in soil but also caused coprecipitation of the two elements on its surface[18], resulting in a significant decrease of soil As content. The main forms of As in the CK group soil were F4 and F5, accounting for 29.5% and 48.4%, respectively. The soil As forms in BC-400, BC-550 and BC-700 were similar but their F5 content was significantly decreased compared with the CK group, by about 12.0, 7.2 and 7.3 mg kg^{-1}, respectively. The phenomenon of residual As decrease was consistent with the findings of Cai et al.[51] and Jiang et al.[52]. Additionally, the content of F4 increased by about 1.1 mg kg^{-1} in the BC-400 group but decreased by about 2.4 mg kg^{-1} in the BC-550 group. This may have been due to the fragmentation of soil particles and a decrease in particle size under an anaerobic environment[53], which meant that the As bound to iron oxides that were encapsulated by other minerals would be released and further transformed. In addition, the contents of F1 increased in the BC groups, particularly in the BC-400 and BC-550 groups, where it rose by approximately 3 and 5 times, respectively. In contrast, Wei et al.[54] conducted a meta-analysis and found that iron-modified biochar reduced the content of F1. The discrepancy suggested that raw biochar might utilize the functional groups to enhance the mobility and repartition of As in soil.

Iron and arsenic loading on biochar

The variations in Fe and As content on biochar differed from those in soil solution and did not show periodic variations with changes between anaerobic to aerobic conditions (Fig. 7). For the three types of biochar, the Fe loading mainly occurred in the first anaerobic period. Additionally, the lower the pyrolysis temperature

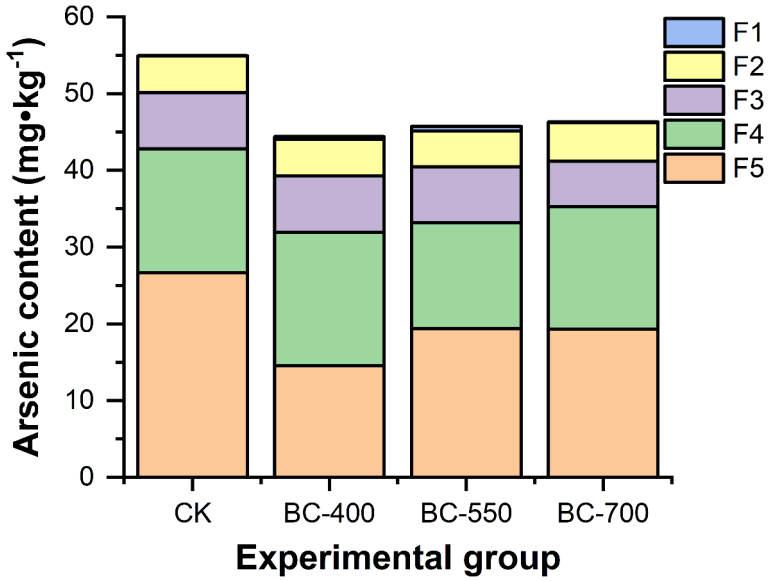

Fig. 6. Content of different arsenic forms in soils across CK, BC-400, BC-550 and BC-700 at the end of the experiment.

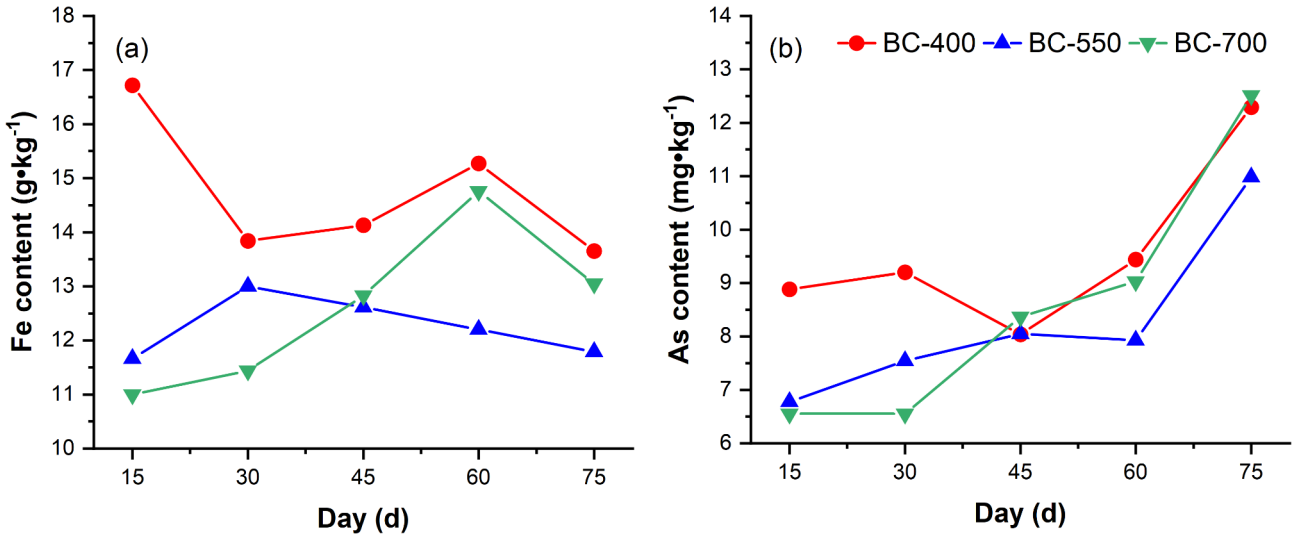

Fig. 7. Changes in (**a**) iron and (**b**) arsenic content on biochar across BC-400, BC-550 and BC-700 over experimental time.

when forming the biochar, the more Fe was loaded. This may have been because biochar prepared at lower temperatures has a greater abundance of functional groups[55], such as -OH, which can bind with $Fe^{[2+}$[56]. The Fe content of biochar in the BC-400 group was relatively high throughout the experiment and showed a decreasing trend over time. This may have been due to the action of dissimilatory iron-reducing bacteria on iron oxides with lower crystallinity (such as ferrihydrite), causing them to detach, similar to iron plaque on rice roots[57]. The other two groups also displayed this phenomenon but at different times. It was also observed that the Fe content of biochar in the BC-550 group was lower than in the other two groups after the second aerobic period (45–60 days). This could be attributed to its lowest relative abundance of Proteobacteria (Fig. 3), which resulted in more Fe(II) remaining in the soil solution (Fig. 4). In contrast to Fe content variation, the amount of As loaded on biochar in each group showed an overall increasing trend over time. This indicated that, although As was mainly combined with iron oxides, the loading capacity of biochar for As did not weaken as the Fe content decreased. The first 30 days were the primary period for biochar to adsorb As, and the As content on biochar was significantly positively correlated with the As concentration in the soil solution ($r = 0.86$, $p < 0.05$). Based on the significant positive correlation between As and Fe concentrations in the soil solution, it was believed that As on biochar primarily originated from the dissolution of As-containing iron oxides.

Surface morphology analysis using SEM showed that the pores were filled after the interaction between biochar and soil and that the minerals therein were in a cemented state (Fig. 8). This was because biochar had a larger specific surface area and higher surface energy, which could promote the aggregation of mineral particles on its pore surface, thereby reducing surface energy. In the high-resolution Fe 2p XPS spectrum of biochar, peaks at 710.40–711.00 eV (Fe 2p3/2) and 723.89–724.32 eV (Fe 2p1/2) were observed (Fig. 8). The single peaks at binding energies of 711.00, 710.40 710.76, 723.89 and 724.32 eV corresponded to Fe_3O_4[58–62] and the peak at 724.30 eV corresponded to FeOOH[63]. The iron oxides carried by biochar had a strong adsorption capacity for As. The characteristic peaks of As(III) at 43.40–43.80 eV were detected on the biochar surface[64,65]. These findings suggested that the biochar mainly adsorbed As(III) on its surface and formed inner-sphere complexes through ligand exchange between arsenite anions and the hydroxyl functional groups of iron (hydr)oxide[66–70]. There was no evidence that Fe(III) oxidised As(III).

Partition analysis of iron and arsenic in soil

As and Fe are closely related in soil and are simultaneously partitioned to soil solution and biochar under flooding conditions. This process is influenced by physiochemical environmental conditions. The As/Fe molar ratio in soil solution exhibited fluctuating characteristics (Fig. 9). Except for the late period for the CK group, the As/Fe molar ratio increased after entering aerobic conditions. This indicated that, although the As and Fe that were released under anaerobic conditions underwent coprecipitation upon the introduction of oxygen, the proportion of As precipitation was relatively low. This suggested that As may have stronger mobility than Fe. It may also be due to the weaker secondary adsorption ability of iron oxides for As under the action of microorganisms[71]. During the experimental process, the As/Fe molar ratio of biochar prepared at different temperatures showed an increasing trend. In the first anaerobic period, the As/Fe molar ratio was lower than that of the soil, which indicated that Fe in soil was more easily partitioned to biochar than As. The gradual increase in the ratio suggested that the adsorption capacity of biochar for As was continuously enhanced (Fig. 7). By the end of the experiment, the As/Fe molar ratio was greater than that of the soil. This further indicated that the partitioning of As from soil to biochar was enhanced, resulting in a larger proportion of As in the soil being

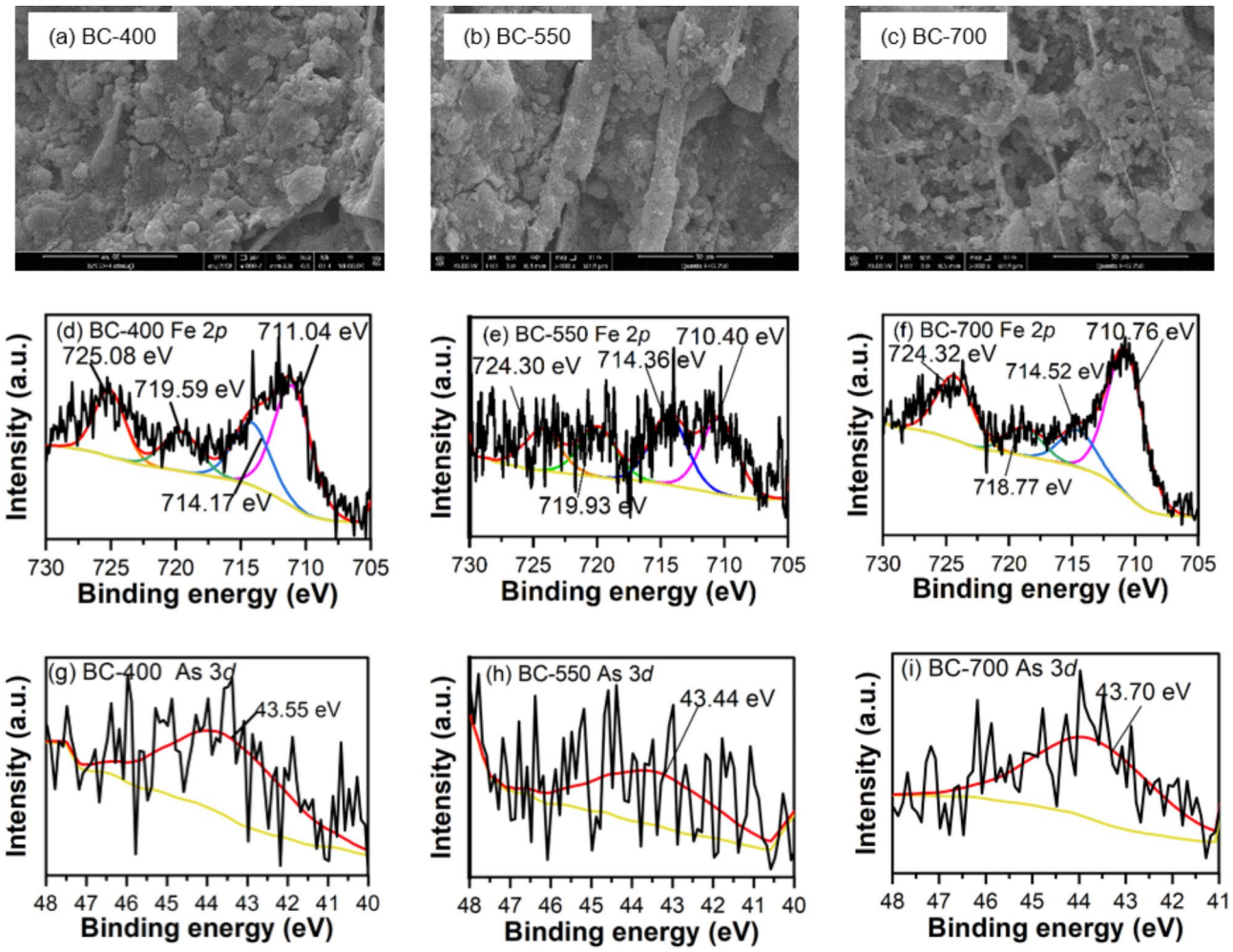

Fig. 8. (**a**–**c**) SEM image and (**d**–**i**) high-resolution Fe2p and As3d XPS spectra of biochar from the BC-400, BC-550 and BC-700 at the end of the experiment.

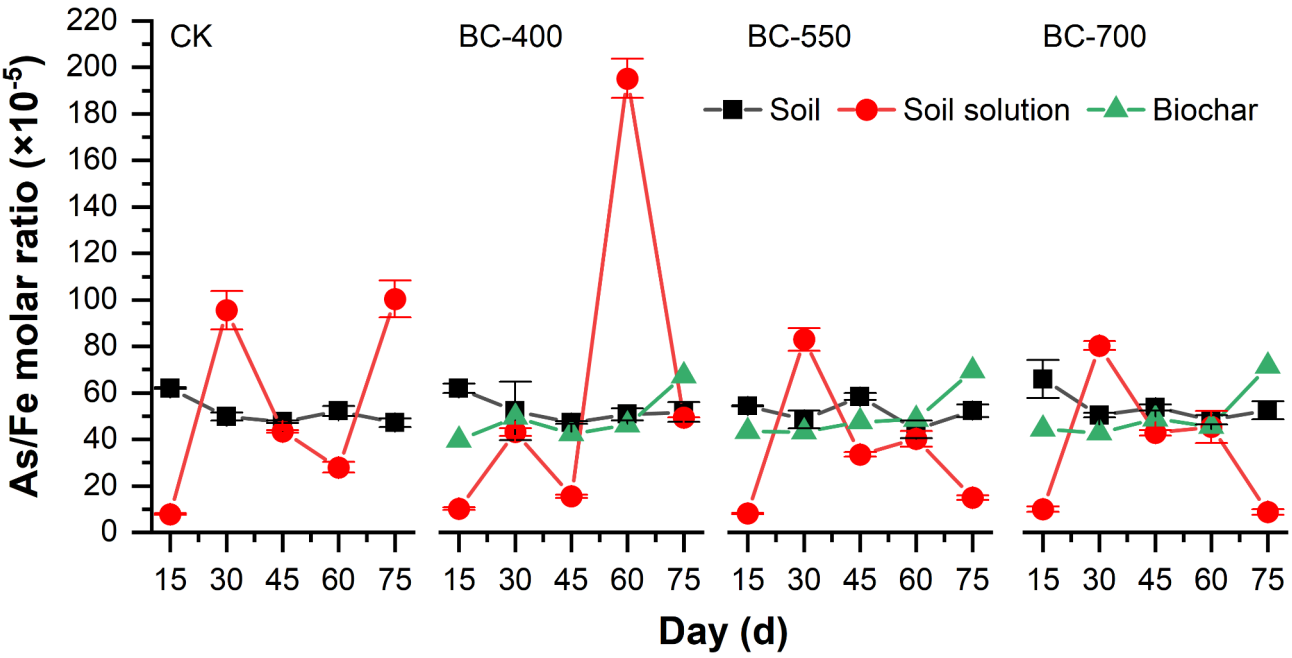

Fig. 9. Molar ratio of As and Fe in soil, soil solution and biochar across CK, BC-400, BC-550 and BC-700 over experimental time.

enriched on biochar. Therefore, it is speculated that when biochar was applied to As-polluted paddy fields, Fe preferentially attached to it and its capacity to load As was enhanced after cycles of wet-drought.

Practical implications

AMD pollution in paddy fields can cause soil acidification and the accumulation of Fe and As. Biochar made from *Eupatorium adenophorum* may help improve contaminated soil. Fe and As will be released and mainly immobilized in the pore structure of biochar as redox conditions fluctuate in paddy fields. Applying biochar prepared at lower temperatures (400 °C and 550 °C) will be more effective in dissolving As-containing iron oxides in soil, while biochar prepared at 400 °C has abundant functional groups and is relatively more stable for immobilizing Fe and As. As trapped in the pores of biochar may not be easily released back into the soil solution under fluctuating redox conditions. The stability of surface As may be influenced by the transformation of iron oxide crystal structure. *Eupatorium adenophorum* is a powerful invasive plant found worldwide, which is both inexpensive and easy to obtain[28]. Using it as feedstock can help reduce the production cost of biochar. After biochar application in paddy fields, grain yield may increase with improvements in soil quality[72]. However, it should be noted that biochar may introduce organic and inorganic contaminants into soil, potentially causing phytotoxicity, cytotoxicity, and neurotoxicity[73]. The microbial population structure in AMD-contaminated fields will change in response to shifts in soil environmental conditions.

Conclusion

Biochar had the potential to remediate AMD-contaminated paddy fields, with its functional groups playing a key role in the process. When prepared at lower pyrolysis temperatures, biochar contained a range of functional groups. In synergy with microorganisms, these functional groups could facilitate the dissolution of As-containing iron oxides produced by AMD, and some of the residual As could also undergo transformation. The dissolved Fe and As in soil solution would be rapidly adsorbed by biochar. Biochar prepared at lower pyrolysis temperatures exhibited a greater capacity to adsorb them, with Fe forming secondary oxides on its surface. While the iron oxides desorbed with fluctuations in redox conditions, the adsorption of As steadily increased. The As/Fe molar ratio on biochar could exceed that of the soil. To be practically applied, field-scale experiments are necessary to further investigate whether the functional groups of biochar degrade and affect the stability of adsorbed Fe and As under repeated wet-dry cycles in paddy fields.

Data availability

The authors declare that the data supporting the findings of this study are available within the paper. Should any raw data files be needed in another format they are available from the corresponding author upon reasonable request.

Received: 31 October 2024; Accepted: 7 February 2025
Published online: 10 February 2025

References

1. Sengupta, S., Bhattacharyya, K., Mandal, J., Bhattacharya, P. & Chattopadhyay, A. P. Zinc and iron enrichment of vermicompost can reduce the arsenic load in rice grain: An investigation through pot and field experiments. *J. Clean. Prod.* **419**, 138267. https://doi.org/10.1016/j.jclepro.2023.138267 (2023).
2. Sun, Y. et al. Long term application of plant growth-promoting bacterium improved grain weight and reduced arsenic accumulation in rice grain: A comparison of 10 bacteria. *Chemosphere* **303**, 135016. https://doi.org/10.1016/j.chemosphere.2022.135016 (2022).
3. Abdul, K. S. M., Jayasinghe, S. S., Chandana, E. P., Jayasumana, C. & De Silva, P. M. C.. Arsenic and human health effects: A review. *Environ. Toxicol. Pharmacol.* **40**, 828–846. https://doi.org/10.1016/j.etap.2015.09.016 (2015).
4. Sharmila, V. G., Tyagi, V. K., Varjani, S. & Banu, J. R. A review on the lignocellulosic derived biochar-based catalyst in wastewater remediation: Advanced treatment technologies and machine learning tools. *Bioresour. Technol.* **387**, 129587. https://doi.org/10.1016/j.biortech.2023.129587 (2023).
5. Yu, X. L. & Lu, S. G. Double effects of biochar in affecting the macropore system of paddy soils identified by high-resolution X-ray tomography. *Sci. Total Environ.* **720**, 137690. https://doi.org/10.1016/j.scitotenv.2020.137690 (2020).
6. Lu, H. L. et al. Effects of the increases in soil pH and pH buffering capacity induced by crop residue biochars on available cd contents in acidic paddy soils. *Chemosphere* **301**, 134674. https://doi.org/10.1016/j.chemosphere.2022.134674 (2022).
7. Vitela-Rodriguez, A. V. & Rangel-Mendez, J. R. Arsenic removal by modified activated carbons with iron hydro(oxide) nanoparticles. *J. Environ. Manag.* **114**, 225–231. https://doi.org/10.1016/j.jenvman.2012.10.004 (2013).
8. Dai, L. C. et al. Tuning oxygenated functional groups on biochar for water pollution control: A critical review. *J. Hazard. Mater.* **420**, 126547. https://doi.org/10.1016/j.jhazmat.2021.126547 (2021).
9. Soares, M. B., Duckworth, O. W., Stýblo, M., Cable, P. H. & Alleoni, L. R. F. Pyrolysis temperature and biochar redox activity on arsenic availability and speciation in a sediment. *J. Hazard. Mater.* **460**, 132308. https://doi.org/10.1016/j.jhazmat.2023.132308 (2023).
10. Zhang, J. et al. Effect and mechanism of biochar as a support on immobilization of different heavy metals by iron oxides in a multi-contaminated soil. *J. Environ. Chem. Eng.* **11**, 109895. https://doi.org/10.1016/J.JECE.2023.109895 (2023b).
11. Xing, Y. et al. Rice hull biochar enhances the mobilization and methylation of mercury in a soil under changing redox conditions: Implication for hg risks management in paddy fields. *Environ. Int.* **168**, 107484. https://doi.org/10.1016/j.envint.2022.107484 (2022).
12. Alozie, N., Heaney, N. & Lin, C. X. Biochar immobilizes soil-borne arsenic but not cationic metals in the presence of low-molecular-weight organic acids. *Sci. Total Environ.* **630**, 1188–1194. https://doi.org/10.1016/j.scitotenv.2018.02.319 (2018).
13. Yang, X. et al. Iron-modified phosphorus- and silicon-based biochars exhibited various influences on arsenic, cadmium, and lead accumulation in rice and enzyme activities in a paddy soil. *J. Hazard. Mater.* **443**, 130203. https://doi.org/10.1016/j.jhazmat.2022.130203 (2023).
14. Shaheen, S. M. et al. Wood-based biochar for the removal of potentially toxic elements in water and wastewater: A critical review. *Int. Mater. Rev.* **64**, 216–247. https://doi.org/10.1080/09506608.2018.1473096 (2019).
15. Wu, C. et al. Effect of sulfur-iron modified biochar on the available cadmium and bacterial community structure in contaminated soils. *Sci. Total Environ.* **647**, 1158–1168. https://doi.org/10.1016/j.scitotenv.2018.08.087 (2019).
16. Tang, X. Y. et al. Use of Fe-impregnated biochar to efficiently sorb chlorpyrifos, reduce uptake by *Allium fistulosum* L., and enhance microbial community diversity. *J. Agric. Food Chem.* **65**, 5238–5243. https://doi.org/10.1021/acs.jafc.7b01300 (2017).
17. Wen, E. G. et al. Iron-modified biochar and water management regime-induced changes in plant growth, enzyme activities, and phytoavailability of arsenic, cadmium and lead in a paddy soil. *J. Hazard. Mater.* **407**, 124344. https://doi.org/10.1016/j.jhazmat.2020.124344 (2021).
18. Hu, L. Y. et al. Immobilization of arsenic in different contaminated soils by zero-valent iron-embedded biochar: Effect of soil characteristics and treatment conditions. *Sci. Total Environ.* **868**, 161597. https://doi.org/10.1016/J.SCITOTENV.2023.161597 (2023).
19. Kumarathilaka, P., Bundschuh, J., Seneweera, S., Marchuk, A. & Ok, Y. S. Iron modification to silicon-rich biochar and alternative water management to decrease arsenic accumulation in rice (*Oryza sativa* L). *Environ. Pollut.* **286**, 117661. https://doi.org/10.1016/j.envpol.2021.117661 (2021).
20. Amen, R. et al. A critical review on arsenic removal from water using biochar-based sorbents: The significance of modification and redox reactions. *Chem. Eng. J.* **396**, 125195. https://doi.org/10.1016/J.JAAP.2022.105542 (2020).
21. Du, T. H., Bogush, A., Mašek, O., Purton, S. & Luiza, C. Campos. Algae, biochar and bacteria for acid mine drainage (AMD) remediation: A review. *Chemosphere* **304**, 135284. https://doi.org/10.1016/j.chemosphere.2022.135284 (2022).
22. Daraz, U., Li, Y., Ahmad, I., Iqbal, R. & Ditta, A. Remediation technologies for acid mine drainage: Recent trends and future perspectives. *Chemosphere* **311**, 137089. https://doi.org/10.1016/j.chemosphere.2022.137089 (2023).
23. Wang, N., Xue, X. M., Juhasz, A. L., Chang, Z. Z. & Li, H. B. Biochar increases arsenic release from an anaerobic paddy soil due to enhanced microbial reduction of iron and arsenic. *Environ. Pollut.* **220**, 514–522. https://doi.org/10.1016/j.envpol.2016.09.095 (2017).
24. Tang, L. et al. Reduced arsenic availability in paddy soil through Fe-organic ligand complexation mediated by bamboo biochar. *Chemosphere* **349**, 140790. https://doi.org/10.1016/j.chemosphere.2023.140790 (2024).
25. Liu, L. C., Sun, P., Chen, Y. Y., Li, X. C. & Zheng, X. L. Distinct chromium removal mechanisms by iron-modified biochar under varying pH: Role of iron and chromium speciation. *Chemosphere* **331**, 138796. https://doi.org/10.1016/j.chemosphere.2023.138796 (2023).
26. Zhang, C. P., Wu, P., Tang, C. Y., Han, Z. W. & Sun, J. Assessment of arsenic distribution in paddy soil and rice plants of a typical karst basin affected by acid mine drainage in southwest China. *Environ. Pollut.* **2**, 27–38. https://doi.org/10.5539/ep.v2n2p27 (2013).
27. Zhang, C. P., Hao, Y. L., Zhang, K. X., Chen, S. & Yang, Z. Y. Effect of biogas slurry and sucrose addition on electrokinetic removal of arsenic from paddy soil. *Int. J. Environ. Sci. Technol.* **20**, 703–714. https://doi.org/10.1007/s13762-022-04006-0 (2023a).
28. Cheng, N., Wang, B., Feng, Q., Zhang, X. & Chen, M. Co-adsorption performance and mechanism of nitrogen and phosphorus onto eupatorium adenophorum biochar in water. *Bioresour. Technol.* **340**, 125696. https://doi.org/10.1016/j.biortech.2021.125696 (2021).
29. Meng, A., Zhang, Y., Zhuo, J., Li, Q. & Qin, L. Investigation on pyrolysis and carbonization of Eupatorium adenophorum Spreng and tobacco stem. *J. Energy Inst.* **88**, 480–489. https://doi.org/10.1016/j.joei.2014.10.003 (2015).
30. Fan, L. Q. et al. Properties of *Eupatorium adenophora* Spreng (Crofton Weed) biochar produced at different pyrolysis temperatures. *Environ. Eng. Sci.* **36**, 937–946. https://doi.org/10.1089/ees.2019.0028 (2019).
31. Liu, F. Z. Study on the influence mechanism of biochar on arsenic migration and transformation in soil-rice system. (Master Thesis) Guizhou University, Guiyang, Guizhou, China. https://doi.org/10.27047/d.cnki.ggudu.2023.000195 (2023).
32. Hu, F. N. et al. Biochar application driven change in soil internal forces improves aggregate stability: Based on a two-year field study. *Geoderma* **403**, 115276. https://doi.org/10.1016/j.geoderma.2021.115276 (2021).
33. Choong, T. S. Y., Chuah, T. G., Robiah, Y., Koay, G. & Azni, F. L. Arsenic toxicity, health hazards and removal techniques from water: An overview. *Desalination* **217**, 139–166. https://doi.org/10.1016/j.desal.2007.01.015 (2007).
34. Chen, S. et al. Biogeochemical transformation of sulfur and its effects on arsenic mobility in paddy fields polluted by acid mine drainage. *Chemosphere* **293**, 133605. https://doi.org/10.1016/j.chemosphere.2022.133605 (2022).

35. Ananyeva, N. D., Susyan, E. A. & Gavrilenko, E. G. Determination of the soil microbial biomass carbon using the method of substrate-induced respiration. *Eurasian Soil. Sci.* **44**, 1215–1221. https://doi.org/10.1134/S1064229311030021 (2011).
36. Hindersmann, I. & Mansfeldt, T. Trace element solubility in a multimetal-contaminated soil as affected by redox conditions. *Water Air Soil Pollut.* **225**, 2158. https://doi.org/10.1007/s11270-014-2158-8 (2014).
37. Lee, D. J., Cheng, Y. L., Wong, R. J. & Wang, X. D. Adsorption removal of natural organic matters in waters using biochar. *Bioresour. Technol.* **260**, 413–416. https://doi.org/10.1016/j.biortech.2018.04.016 (2018).
38. Cisternas, J., Rodríguez, C., Serrano, J. & Leiva, E. Study of the key biotic and abiotic parameters influencing ammonium removal from wastewaters by Fe^{3+}-mediated anaerobic ammonium oxidation (feammox). *Chemosphere* **339**, 139463. https://doi.org/10.1016/J.CHEMOSPHERE.2023.139463 (2023).
39. Zhang, G. G., Liu, X. W., Gao, M. L. & Song, Z. G. Effect of Fe–Mn–Ce modified biochar composite on microbial diversity and properties of arsenic-contaminated paddy soils. *Chemosphere* **250**, 126249. https://doi.org/10.1016/j.chemosphere.2020.126249 (2020).
40. Dangeti, S. et al. Microbial communities and biogenic Mn-oxides in an on-site biofiltration system for cold Fe-(II)- and mn(II)-rich groundwater treatment. *Sci. Total Environ.* **710**, 136386. https://doi.org/10.1016/j.scitotenv.2019.136386 (2020).
41. Revesz, E., Fortin, D. & Paktunc, D. Reductive dissolution of arsenical ferrihydrite by bacteria. *Appl. Geochem.* **66**, 129–139. https://doi.org/10.1016/j.apgeochem.2015.12.007 (2016).
42. Chia, C. H. et al. Imaging of mineral-enriched biochar by FTIR, Raman and SEM-EDX. *Vib. Spectrosc.* **62**, 248–257. https://doi.org/10.1016/j.vibspec.2012.06.006 (2012).
43. Zeng, H. T. et al. Efficient adsorption of cr (VI) from aqueous environments by phosphoric acid activated eucalyptus biochar. *J. Clean. Prod.* **286**, 124964. https://doi.org/10.1016/j.jclepro.2020.124964 (2021).
44. Zhou, C. L., Song, X., Wang, Y. W., Wang, H. & Ge, S. F. The sorption and short-term immobilization of lead and cadmium by nano-hydroxyapatite/biochar in aqueous solution and soil. *Chemosphere* **286**, 131810. https://doi.org/10.1016/j.chemosphere.2021.131810 (2022).
45. Liu, C., Chen, L., Ding, D. & Cai, T. From rice straw to magnetically recoverable nitrogen doped biochar: Efficient activation of peroxymonosulfate for the degradation of metolachlor. *Appl. Catal. B Environ.* **254**, 312–320. https://doi.org/10.1016/j.apcatb.2019.05.014 (2019).
46. Chen, M., He, F., Hu, D., Bao, C. & Huang, Q. Broadened operating pH range for adsorption/reduction of aqueous cr(VI) using biochar from directly treated jute (*Corchorus capsularis* L.) fibers by H_3PO_4. *Chem. Eng. J.* **381**, 122739. https://doi.org/10.1016/j.cej.2019.122739 (2020).
47. He, J., Xiao, Y., Tang, J., Chen, H. & Sun, H. Persulfate activation with sawdust biochar in aqueous solution by enhanced electron donor-transfer effect. *Sci. Total Environ.* **690**, 768–777. https://doi.org/10.1016/j.scitotenv.2019.07.043 (2019).
48. Kappler, A. et al. Biochar as an electron shuttle between bacteria and Fe(III) minerals. *Environ. Sci. Technol. Lett.* **1**, 339–344. https://doi.org/10.1021/ez5002209 (2014).
49. Xu, S. et al. Biochar facilitated microbial reduction of hematite. *Environ. Sci. Technol.* **50**, 2389–2395. https://doi.org/10.1021/acs.est.5b05517 (2016).
50. Yuan, H. J. et al. Biochar's role as an electron shuttle for mediating soil N_2O emissions. *Soil. Biol. Biochem.* **133**, 94–96. https://doi.org/10.1016/j.soilbio.2019.03.002 (2019).
51. Cai, X. L. et al. Biogeochemical processes of arsenic transformation and redistribution in contaminated soils: Combined effects of iron, sulfur, and organic matter. *Geoderma* **422**, 115948. https://doi.org/10.1016/J.GEODERMA.2022.115948 (2022).
52. Jiang, F. et al. Effect of ascorbic acid and combination with fulvic acid on the electrokinetic remediation of paddy soil contaminated by arsenic-containing acid mine drainage. *Appl. Geochem.* **152**, 105632. https://doi.org/10.1016/j.apgeochem.2023.105632 (2023).
53. Li, R. Y. et al. Study on the phase transformation of iron oxides in metallurgically contaminated soil under water incubation. *Environ. Sci. Technol.*. https://link.cnki.net/urlid/42.1245.X.20230803.1707.002 (2023) (in Chinese).
54. Wei, B. L. et al. Iron-modified biochar effectively mitigates arsenic-cadmium pollution in paddy fields: A meta-analysis. *J. Hazard. Mater.* **469**, 133866. https://doi.org/10.1016/j.jhazmat.2024.133866 (2024).
55. Aktar, S. et al. Effects of temperature and carrier gas on physicochemical properties of biochar derived from biosolids. *J. Anal. Appl. Pyrol.* **164**, 105542. https://doi.org/10.1016/J.JAAP.2022.105542 (2022).
56. Sema, A. & Bhattacharyya, J. Biochar derived from waste bamboo shoots for the biosorptive removal of ferrous ions from aqueous solution. *J. Indian Chem. Soc.* **99**, 100791. https://doi.org/10.1016/J.JICS.2022.100791 (2022).
57. Zhou, H. et al. Cadmium uptake, accumulation, and remobilization in iron plaque and rice tissues at different growth stages. *Ecotoxicol. Environ. Saf.* **152**, 91–97. https://doi.org/10.1016/j.ecoenv.2018.01.031 (2018).
58. Wu, L. P., Zhang, S. R., Wang, J. & Ding, X. D. Phosphorus retention using iron (II/III) modified biochar in saline-alkaline soils: Adsorption, column and field tests. *Environ. Pollut.* **261**, 114223. https://doi.org/10.1016/j.envpol.2020.114223 (2020).
59. Li, J. et al. A study of modified Fe_3O_4 nanoparticles for the synthesis of ionic ferrofluids. *Appl. Surf. Sci.* **256**, 6977–6981. https://doi.org/10.1016/j.apsusc.2010.05.009 (2010).
60. Balachandramohan, J., Anandan, S. & Sivasankar, T. A simple approach for the sonochemical synthesis of Fe_3O_4-guargum nanocomposite and its catalytic reduction of p-nitroaniline. *Ultrason. Sonochem.* **40**, 1–10. https://doi.org/10.1016/j.ultsonch.2017.06.012 (2018).
61. Banerjee, Y. B. et al. Preparation of γ-Fe_2O_3 nanoparticles using DC thermal arc-plasma route, their characterization and magnetic properties. *Scr. Mater.* **54**, 1235–1240. https://doi.org/10.1016/j.scriptamat.2005.12.029 (2006).
62. Qamar, S. A. et al. Alginate-based nano-adsorbent materials-Bioinspired solution to mitigate hazardous environmental pollutants. *Chemosphere* **288**, 132618. https://doi.org/10.1016/j.chemosphere.2021.132618 (2022).
63. Park, J. H., Wang, J. J. & Seo, D. C. Comparison of catalytic activity for treating recalcitrant organic pollutant in heterogeneous Fenton oxidation with iron-impregnated biochar and activated carbon. *J. Water Process. Eng.* **42**, 102141. https://doi.org/10.1016/j.jwpe.2021.102141((2021).
64. Chen, J. Z. et al. Extracellular polymeric substances and mineral interfacial reactions control the simultaneous immobilization and reduction of arsenic (as(V)). *J. Hazard. Mater.* **456**, 131651. https://doi.org/10.1016/j.jhazmat.2023.131651 (2023).
65. Kim, J. W., Song, J. Y., Lee, S. M. & Jung, J. H. Application of iron-modified biochar for arsenite removal and toxicity reduction. *J. Ind. Eng. Chem.* **80**, 17–22. https://doi.org/10.1016/j.jiec.2019.07.026 (2019).
66. Raul, P. K. et al. Iron oxide hydroxide nanoflower assisted removal of arsenic from water. *Mater. Res. Bull.* **49**, 360–368. https://doi.org/10.1016/J.MATERRESBULL.2013.09.015 (2014).
67. Zhang, S. X., Niu, H. Y., Cai, Y. Q., Zhao, X. L. & Shi, Y. L. Arsenite and arsenate adsorption on coprecipitated bimetal oxide magnetic nanomaterials: $MnFe_2O_4$ and $CoFe_2O_4$. *Chem. Eng. J.* **158**, 599–607. https://doi.org/10.1016/j.cej.2010.02.013 (2010).
68. Iakovleva, E. et al. Modified and unmodified low-cost iron-containing solid wastes as adsorbents for efficient removal of as(III) and as(V) from mine water. *J. Clean. Prod.* **133**, 1095–1104. https://doi.org/10.1016/j.jclepro.2016.05.147 (2016).
69. Mahmood, T., Aslam, M., Naeem, A., Siddique, T. & Din, S. U. Adsorption of as(III) from aqueous solution onto iron impregnated used tea activated carbon: Equilibrium, kinetic and thermodynamic study. *J. Chil. Chem. Soc.* **63**, 3855. https://doi.org/10.4067/s0717-97072018000103855 (2018).
70. Yang, J. S., Kim, Y. S., Park, S. M. & Baek, K. Removal of as(III) and as(V) using iron-rich sludge produced from coal mine drainage treatment plant. *Environ. Sci. Pollut Res.* **21**, 10878–10889. https://doi.org/10.1007/s11356-014-3023-4 (2014).
71. Zhang, Z. N., Yin, N. Y., Du, H. L., Cai, X. L. & Cui, Y. S. The fate of arsenic adsorbed on iron oxides in the presence of arsenite-oxidizing bacteria. *Chemosphere* **151**, 108–115. https://doi.org/10.1016/j.chemosphere.2016.02.065 (2016).

72. He, X. L., Yang, Y. R., Huang, B. S., Wang, Z. H. & Wang, M. X. An overview of characteristic factors of biochar as a soil improvement tool in rice growth-A review. *Environ. Res.* **242**, 117794. https://doi.org/10.1016/j.envres.2023.117794 (2024).
73. Han, H. W. et al. Contaminants in biochar and suggested mitigation measures—a review. *Chem. Eng. J.* **429**, 132287. https://doi.org/10.1016/j.cej.2021.132287 (2022).

Acknowledgements
The authors wish to express their thanks for the financial support of the National Natural Science Foundation of China (No. U1612442), the Project of Basic Research of Guizhou Province (No. ZK[2024]016), and the Project of Science and Technology Department of Guizhou Province (No. GCC[2023]045, No. LH[2024]029).

Author contributions
C.Z.: Conceptualization, Writing-Original draft preparation, Writing- Reviewing and Editing. J.L.: Methodology, Investigation. W.S.: Visualization. Han Chen: Visualization. S.Z.: Formal analysis.

Declarations

Competing interests
The authors declare no competing interests.

Additional information
Correspondence and requests for materials should be addressed to C.Z.

Reprints and permissions information is available at www.nature.com/reprints.

Publisher's note Springer Nature remains neutral with regard to jurisdictional claims in published maps and institutional affiliations.